



3 4456 0054066 2

ORNL/SUB/83-51926/2

MILLIMETER WAVE DIELECTRIC PROPERTY MEASUREMENT OF GYROTRON WINDOW MATERIALS

TECHNICAL REPORT FOR THE PERIOD
January 26, 1983 through October 31, 1984
(Rockwell Report No. SC5357.4FR)

FED LIBRARY SEP 16 1985

W.W. HO

APRIL 1985

FUSION ENERGY DIVISION LIBRARY

Report prepared by

ROCKWELL INTERNATIONAL SCIENCE CENTER
1049 Camino Dos Rios
Thousand Oaks, CA 91360

Under

Subcontract Purchase Order No. 11Y-51926C

For

OAK RIDGE NATIONAL LABORATORY
Oak Ridge, Tennessee 37831

Operated by

MARTIN MARIETTA ENERGY SYSTEMS, INC.
for the
U.S. DEPARTMENT OF ENERGY
Under Contract No. DE-AC05-84OR21400

This report was prepared as an account of work sponsored by an agency of the United States Government. Neither the United States Government nor any agency thereof, nor any of their employees, makes any warranty, expressed or implied, or assumes any legal liability or responsibility for the accuracy, completeness, or usefulness of any information, apparatus, product, or process disclosed, or represents that its use would not infringe privately owned rights. Reference herein to any specific commercial product, process, or service by trade name, trademark, manufacturer, or otherwise, does not necessarily constitute or imply its endorsement, recommendation, or favoring by the United States Government or any agency thereof. The views and opinions of the authors expressed herein do not necessarily state or reflect those of the United States Government or any agency thereof.

MARTIN MARIETTA ENERGY SYSTEMS LIBRARIES



3 4456 0054066 2



TABLE OF CONTENTS

	<u>Page</u>
1.0 ABSTRACT.....	1
2.0 SUMMARY.....	2
3.0 EXPERIMENTAL METHOD.....	6
4.0 EXPERIMENTAL RESULTS.....	8
4.1 Single Crystal Sapphire.....	8
4.2 Commercial Polycrystalline Alumina.....	12
4.3 Exploratory Alumina Formulations.....	14
4.4 Zirconia-Toughened Alumina.....	16
4.5 Low-Loss Fluids.....	20
4.6 Chemical and Microstructural Analysis.....	23
5.0 CONCLUSIONS AND RECOMMENDATIONS.....	41
6.0 REFERENCES.....	44



LIST OF FIGURES

	<u>Page</u>
Fig. 1 Summary of room temperature millimeter-wave measurement results for the loss tangent of single crystal sapphire and various polycrystalline Al_2O_3 samples.....	11
Fig. 2 Measured room temperature dielectric constant values at 35 GHz for $ZrO_2-Al_2O_3$ samples as a function of ZrO_2 concentration.....	19
Fig. 3 Measured room temperature loss tangent values at 35 GHz for $ZrO_2-Al_2O_3$ samples as a function of ZrO_2 concentration...	19
Fig. 4 Measured dielectric constant values for low-loss fluids as a function of temperature.....	23
Fig. 5 Glassy triple points in Coors-AD-995 alumina.....	26
Fig. 6 Bright field, dark field pair of a glassy triple point and surrounding grain boundaries in Coors AD-995.....	27
Fig. 7 Bright field micrograph of the microstructure of Ampex 995 showing the absence of any boundary phase.....	29
Fig. 8 Bright field micrograph of the microstructure of the Union Carbide hot-pressed Al_2O_3 showing the presence of small voids.....	30
Fig. 9 Bright field micrograph from the Union Carbide Al_2O_3 showing the triangular holes at the grain corners.....	31
Fig. 10 Bright field micrograph from the Union Carbide Al_2O_3 showing the faint diffraction contrast from the grain junction.....	32
Fig. 11 (a) SEM of ultra-high purity Al_2O_3 sample fabricated at the Science Center by hot isostatic pressing; (b) SEM of ORNL fine grain Al_2O_3 sample.....	34
Fig. 12 (a) SEM of hot isostatically pressed Al_2O_3 sample containing TiO_2 as densification aid fabricated at the Science Center; (b) elemental x-ray mapping by EDAX showing distribution of Ti within sample illustrated by (a).....	35



LIST OF FIGURES

	<u>Page</u>
Fig. 13 Microprobe chemical analysis by EDAX of fractured surface for ORNL $ZrO_2-Al_2O_3$ sample ALZRY 19-4.....	36
Fig. 14 (a) SEM of fractured surface of ORNL $ZrO_2-Al_2O_3$ sample ALZRY 19-4 showing inclusions; (b) elemental x-ray mapping by EDAX showing distribution of Fe within sample illustrated in (a).....	38
Fig. 15 SEM showing the distribution of ZrO_2 (white) in Al_2O_3 matrix for ORNL sample ALZRY 19-4.....	39
Fig. 16 (a) SEM showing the distribution of ZrO_2 (white) in Al_2O_3 matrix for ORNL sample ALZRY 20-5; (b) SEM showing the distribution of ZrO_2 (white) in Al_2O_3 matrix for ORNL sample ALZRY 28-1.....	40



LIST OF TABLES

	<u>Page</u>
Table 1 Measured Room Temperature (23°C) Dielectric Properties of Single Crystal Sapphire Manufactured by Crystal Systems, Inc.....	10
Table 2 Measured Room Temperature (23°C) Dielectric Properties of Commercial Polycrystalline Al ₂ O ₃ Samples.....	13
Table 3 Measured Room Temperature (23°C) Dielectric Properties of ZrO ₂ -Al ₂ O ₃ Materials at 35 GHz.....	15
Table 4 Measured Room Temperature (23°C) Dielectric Properties of Zirconia-Alumina Materials at 35 GHz.....	18
Table 5 Measured Room Temperature (23°C) Dielectric Properties of Low-Loss Fluids at 8.4 GHz.....	22
Table 6 Measured Dielectric Properties of Low-Loss Fluids at 35 GHz as Function of Temperature.....	22
Table 7 Measured Room Temperature (20°C) Dielectric Loss at 100 GHz and Viscosity Data for Normal Alkanes as Obtained from Literature.....	24

1.0 ABSTRACT

The objectives of this program are to determine the millimeter-wave dielectric properties of various single crystal and ceramic materials and coolant fluids to provide the database for assessing their potentials and limitations in high power gyrotron window applications. Chemical and microstructural analyses are carried out on material systems showing the most promise for correlation of dielectric properties with material properties, and for establishing key processes and parameters controlling millimeter-wave absorption in support of advanced materials development efforts.

2.0 SUMMARY

This final report presents the results obtained for the program, "Millimeter-Wave Dielectric Property Measurement of Gyrotron Window Materials," under the sponsorship of Martin Marietta Subcontract No. 11Y-51926C. The period of performance of this effort extends from 01/26/83 through 10/31/84. The scope, experimental techniques employed, and the measurement results obtained in the first-year effort over the period 01/26/83 to 02/29/84 have been described in detail in the previous technical report, "Millimeter-Wave Dielectric Property Measurement of Gyrotron Window Materials," ORNL/SUB/83-51926/1, Rockwell Report No. SC5357.2TR. The current report is devoted primarily to the results from the technical effort over the subsequent time period 03/01/84 through 10/31/84.

In the previous technical report (ORNL/SUB/83-51926/1), dielectric properties of various standard and advanced window materials and a series of fluorocarbon fluids were presented in tabular and graphic format. The window materials studied included: various commercial grade alumina (Coors AD-995, Coors AD-999 and Wesgo AL-995); fine-grain hot-pressed alumina (fabricated by ORNL), standard optical grade single crystal sapphire (Crystal System Hemlite); aluminum oxynitride (Raytheon); magnesium aluminum spinel (Raytheon); beryllium oxide (ORNL); and sintered silicon nitride (GT&E AY6 and PY6). The fluorocarbon fluids characterized included 3M Corporation, Fluorinert FC-43, FC-75 and FC-104, respectively. Details of these results and of those for chemical and microstructural analysis carried out on the alumina samples may be found by referring to the previous report.

In the technical effort during the period of performance 03/01/84 through 10/31/84, a detailed systematic investigation was carried out to establish the millimeter-wave dielectric properties of single crystal sapphire as a function of frequency (30-140 GHz), crystal orientation and sample quality. Measurements were carried out on samples ranging from the lowest optical grade (Crystal System Hemcore) to the best obtainable grade (Crystal System

Hemex). This effort was aimed at establishing the intrinsic dielectric loss in sapphire and at understanding the mechanisms and processing parameters giving rise to additional extrinsic dielectric loss in ceramic Al_2O_3 . Within this context, measurements for a number of the ceramic Al_2O_3 previously studied were extended to 140 GHz, and several new commercial formulations were tested. These results were compared to the sapphire data in terms of absolute magnitude of loss, as well as relative frequency dependences. These data, together with detailed chemical and microstructural studies carried out on select Al_2O_3 samples, were used to obtain information on the effects of impurities, porosity, grain size and size distribution, secondary and intergranular phases, and grain boundary properties on the dielectric loss in ceramic Al_2O_3 .

Since fracture toughness and resistance to long-term fatigue failure are key requirements in gyrotron window applications, an exploratory program was carried out on the ceramic $\text{ZrO}_2\text{-Al}_2\text{O}_3$ material system. The addition of various concentrations of ZrO_2 to Al_2O_3 has been shown to control grain growth and thus to minimize the presence of bimodal distributions in grain size, as well as to improve the material's fracture toughness. This latter phenomenon is achieved via transformation toughening, whereby mechanical stresses induce a phase change in the ZrO_2 grains from tetragonal structures to monoclinic, with an accompanying volume expansion of about 3%. This expansion generates compressive stresses which will minimize strength degradation due to surface cracks and flaws. To determine the feasibility of using this material system in gyrotron window applications, the millimeter-wave dielectric properties of a series of samples with ZrO_2 concentrations up to 60% fabricated at Rockwell Science Center and Oak Ridge National Laboratory were measured. In addition, two samples of partially stabilized zirconia (PSZ) manufactured by Nilcra Ceramics, Inc. were characterized. The primary purposes of this investigation were to establish trends in the changes of dielectric properties as a function of ZrO_2 concentration, and to compare its expected performance to single crystal sapphire and ceramic Al_2O_3 .

SC5357.4FR

The dielectric properties of a series of low-loss candidate cooling fluids were also studied. These fluids were chosen by TRW, Inc., as alternatives to the previously characterized fluorocarbon fluids in gyrotron window cooling applications, based on their higher flash temperature and lower potential health hazard in combustion. The purpose of this task was to expand the database for the millimeter-wave properties of low loss fluids so that choices will be available to designers of high power gyrotron windows to meet specific system performance criteria.

The measurement results obtained for sapphire indicated that their loss tangents are significantly lower than any ceramic material over the frequency range 30-140 GHz. Dielectric properties along the principal crystal axes were found to be independent of the optical grades of the samples studied. Preliminary indications show that the millimeter-wave losses will be further reduced at cryogenic temperatures.

The best commercial alumina materials (Coors AD-995, Ampex 99.5%, Ampex 99.9%) are a factor of two to three times more absorbing than sapphire. In-depth analysis of the chemical and microstructural properties of a series of commercial and specially formulated alumina samples with widely varying dielectric properties have established that impurities occurring within individual grains of alumina are prime contributors to the millimeter-wave loss. They are more likely to occur in fine-grained materials and in formulations with high initial concentrations of additives. These restrictions make very difficult the task of developing high strength, low absorption alumina materials, and further developmental efforts are required before the performance of the best commercial aluminas can be exceeded.

Measured high dielectric constants for the $ZrO_2-Al_2O_3$ material system restrict their usefulness in window applications to compositions with ZrO_2 below 15 v/o. The loss tangents, however, are excessively high, even in this concentration range for the samples studied. Whether the improved strength properties (30-50%) are entirely offset by the degradation in loss properties,



SC5357.4FR

and whether these losses can be reduced by suitable control of microcrystalline properties are yet to be determined.

The alkane fluids proved to have absorptions far lower than the organic oils and the fluorocarbon fluids. The range of physical properties available for this group of fluid (viscosity, flash temperature, heat capacity, etc.) makes them attractive as alternative candidates to the fluorocarbon fluids in cooling applications.

3.0 EXPERIMENTAL METHOD

The millimeter-wave dielectric properties of solid samples were determined either by a free-wave transmission and reflection method or by a cavity perturbation method. In the former case, a plane parallel sample is placed in the path of either a collimated or a focused microwave beam. The dielectric properties are then deduced from the power reflection and transmission coefficients and their variation with frequency, and the thickness of the sample. In the latter case, where large samples are not available and for liquids, a rod sample or a cylindrical tube containing the fluid under measurement is placed inside a resonant cavity structure. The dielectric constant and loss tangent of the sample are then calculated from the measured resonant frequency and the change in quality factor (Q) of the cavity response. These methods have been described in previous reports where the experimental technique, calibration procedure and measurements results on a wide variety of materials over the frequency range 30-110 GHz and temperature range up to 1600°C were discussed in detail.^{1,2} One major improvement made for the current program was the extension of the measurements to 140 GHz. This consisted primarily of adding suitable power sources, horns and antennas and other millimeter-wave components, and of redesigning the experimental setup to allow for better alignment to meet the more stringent tolerance requirements imposed by the shorter wavelength. This enhanced capability allowed measurements to be performed in the 130-140 GHz frequency range in anticipation of future higher frequency dielectric characterization requirements in the gyrotron development program.

Materials properties measurements were carried out with a variety of standard and advanced analyses methods, including x-ray diffraction (XRD), scanning electron microscopy (SEM), scanning transmission electron microscopy (STEM), energy dispersive x-ray analysis (EDAX), and microprobe analysis. These methods were used on select samples to determine their microstructure



SC5357.4FR

and composition, and the presence, location and chemical state of minor and trace elements. Emphasis was placed on correlation of basic materials properties with dielectric properties to obtain a more fundamental understanding of the mechanisms governing the dielectric loss in ceramic materials.

4.0 EXPERIMENTAL RESULTS

4.1 Single Crystal Sapphire

A detailed millimeter-wave dielectric properties characterization program was carried out on single crystal sapphire over the frequency range 30-140 GHz. The objectives for this task are to establish the intrinsic dielectric loss in sapphire and to determine the degradation caused by crystal imperfections such as air bubble content, and crystal defects and impurities. The data will also determine the ultimate achievable values for loss in Al_2O_3 ceramic material in general.

For these purposes, measurements were carried out on sapphire samples of different optical quality, ranging from the lowest optical grade (Crystal System Hemcore) to the best obtainable grade (Crystal System Hemex). Samples were fabricated in sufficiently large sizes (approximately 7.75 cm in diameter and 5 cm thick) to provide the necessary measurement accuracy for use with the free-space transmission and reflection measurement method. In addition, for each of the Hemcore and Hemex grade, two different samples, one with the sample face parallel to the crystal optical axis (a-cut) and one with the sample face perpendicular to the optical axis (c or z-cut), were used. When the sample face is perpendicular to the direction of electromagnetic wave propagation, the c-cut crystal will exhibit isotropic dielectric properties for rotations about the crystal axis. This orientation is commonly referred to as $E \perp c$, where the electric field of the incoming radiation is perpendicular to the optical or c-axis. For the a-cut sample, both the a- and c-axes will be in the plane defined by the face of the sample. A linearly polarized electromagnetic wave normally incident on the sample, depending on the rotational orientation of the sample, will have its electric field vector aligned parallel or perpendicular to the crystal c-axis. Consequently, use of a- and c-cut samples together allows complete determination of the dielectric properties of single crystal sapphire for orientations of the electric field both parallel and perpendicular to the crystal c-axis, as well as a redundancy check for the latter case.

SC5357.4FR

The results obtained are given in Table 1. To within the quoted experimental uncertainties, the results for the dielectric constant and the loss tangents are virtually identical for the two grades of sapphire. Consequently, differences in optical quality in the sample studied (mainly air bubble content and crystal defects) are not significant in terms of millimeter-wave dielectric properties. Since the cost for Hemex grade sapphire is several times that for Hemcore grade sapphire, this conclusion can potentially lead to substantial savings if sapphire becomes the preferred choice in millimeter-wave gyrotron window applications.

For comparison, loss tangents for sapphire in the E1c orientation obtained in the current work are shown as a function of frequency in Fig. 1, together with the various earlier low frequency (8-9 GHz) results reported by Westphal et al^{3,4} and the continuous high frequency (100-400 GHz) results obtained by Afsar and Button⁵ using dispersive Fourier transform spectroscopy techniques. Also shown are results of model calculations of Slack⁶ based on experimental fits to the IR spectra and extrapolation to the low frequency wings of the IR band. Current data can be seen to have the same general frequency dependence as predicted by Slack, but is approximately a factor of 3 higher in magnitude. It is also approximately a factor of 2 lower than the experimental data of Afsar and Button, which were obtained on nominally the same type of sapphire sample (Crystal System Hemlite). Low frequency results are sufficiently uncertain that they do not enable discrimination of the high frequency data sets. This discrepancy between the current work and the data of Afsar and Button is apparently present only in sapphire, since comparisons of the Wesgo AL-995 and Coors AD-999 data showed good agreement, as shown in Fig. 1. A detailed review of current data for sapphire failed to uncover any possible source of systematic error which might have been overlooked. In fact, most effects considered would tend to lower the loss value, making the disagreement even more apparent.

Table 1
 Measured Room Temperature (23°C) Dielectric Properties of Single
 Crystal Sapphire Manufactured by Crystal Systems, Inc.

Sample Type & Orientation	Thickness (cm)	Density (gm/cc)	30-40 GHz		55-60 GHz		90-100 GHz		130-140 GHz	
			k (±0.006)	tan δ (X10 ⁻³)	k (±0.005)	tan δ (X10 ⁻³)	k (±0.003)	tan δ (X10 ⁻³) (±5)	k (±0.002)	tan δ (X10 ⁻³) (±5)
Hemcore, c-cut: E1c	5.0902	3.980	9.392	< 10	9.392	< 10	9.391	15	9.385	20
Hemcore, a-cut: E1c	5.0902	3.980	9.392	< 10	9.392	< 10	9.391	12	9.389	23
			E11c	11.585	< 10	11.585	< 10	11.580	16	11.578
Hemex, c-cut: E1c	5.0846	3.981	9.390	< 10	9.390	< 10	9.389	11	9.388	14
Hemix, a-cut: E1c	5.0825	3.980	9.390	< 10	9.389	< 10	9.388	13	9.387	17
			E11c	11.582	< 10	11.580	< 10	11.577	16	11.576

C6795A/sn
10

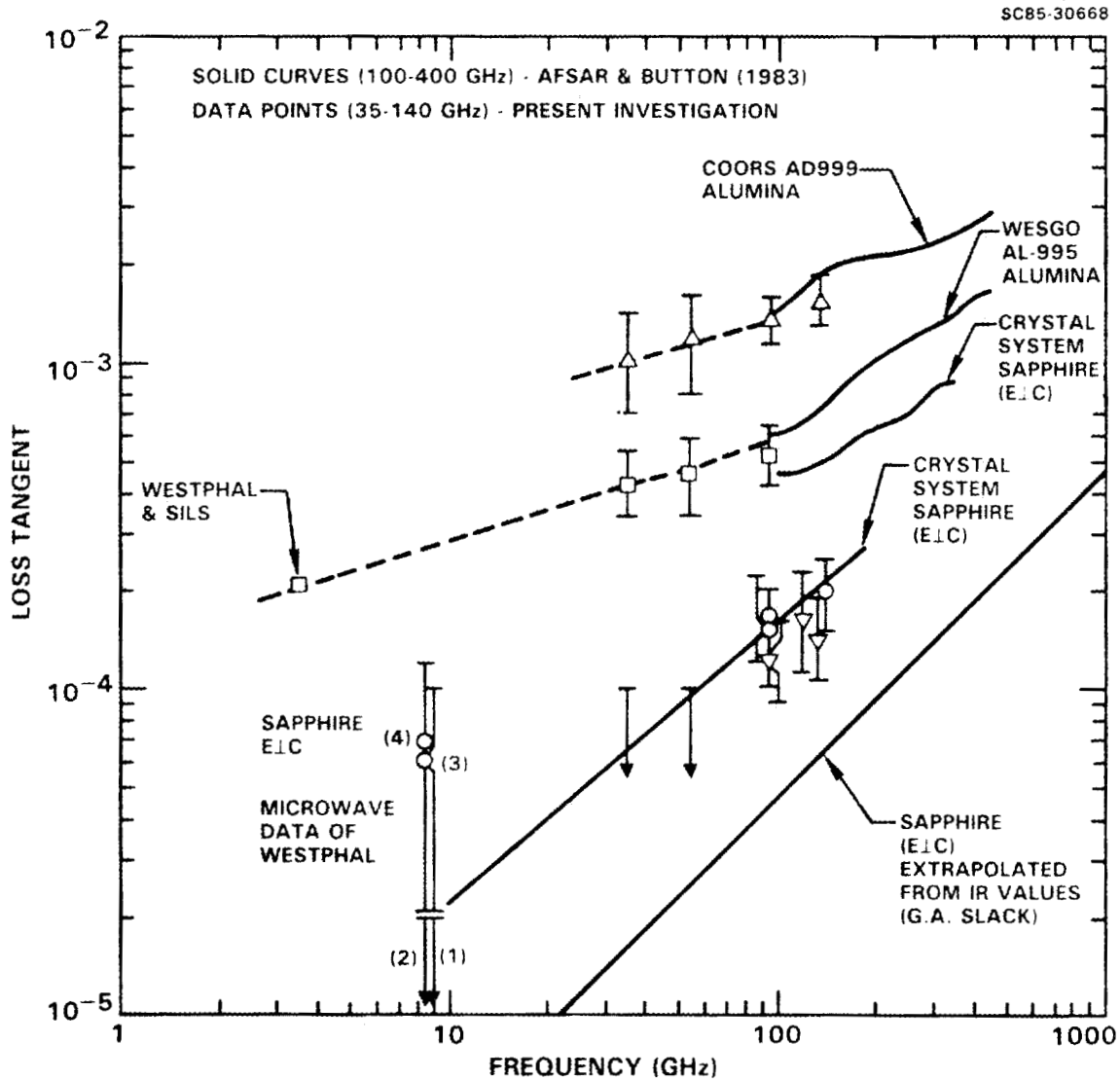


Fig. 1 Summary of room temperature millimeter-wave measurement results for the loss tangent of single crystal sapphire and various polycrystalline Al_2O_3 samples.

The agreement obtained for the loss tangent in the different grades of sapphire studied indicated that sample quality is not a significant issue. The self-consistency obtained for the loss tangents as measured in the a- and c-cut samples indicated that polarization effects were not present in the current experiment. The error bars shown in Fig. 1 represent the best estimate

of the total uncertainty from random and systematic errors in the measurements. Since sapphire to date has been shown to possess the lowest loss tangent in candidate window materials, establishment of the absolute magnitude of the loss in the millimeter-wave region of interest is critical in the overall materials characterization and development program aimed at gyrotron window applications. A strong recommendation is that further efforts be undertaken to resolve this apparent discrepancy.

4.2 Commercial Polycrystalline Alumina

Dielectric characterizations were also carried out on disk Al_2O_3 samples, using the free-wave measurement method. They consisted of 130-140 GHz measurements of Al_2O_3 samples previously studied up to 100 GHz (Coors AD-995, Coors AD-999 and Ampex 99.5%) and still available for further testing, and a new high purity 99.9% sintered Al_2O_3 sample manufactured by Ampex (Ampex 99.9%). The data obtained, together with low frequency results for the two samples previously studied, are shown in Table 2. The Ampex 99.9%, Ampex 99.5% and Coors AD-995 (99.5%) samples exhibited similar loss characteristics throughout the entire frequency range, while the Coors AD-999 sample showed losses which were consistently a factor of 4 higher. The analysis of the starting powder for the Ampex 99.9% sample before firing indicated that the total impurity concentration was below 0.05%, with the breakdown as follows: silica = 0.012%; CaO = 0.008%; NaO = 0.008%; BaO = 0.004%; Fe_2O_3 = 0.003%; all other impurities < 0.001%. A hydrocarbon binder is used to constitute the powder which is expected to be completely volatilized during sintering. Although measurement uncertainties are large by comparison, there is some indication that the lower observed loss in the Ampex 99.9% material reflects the higher purity of the material. A more detailed discussion regarding distribution of impurities and their effect on dielectric properties for these materials is given in Section 4.6.

Table 2
 Measured Room Temperature (23°C) Dielectric Properties of Commercial
 Polycrystalline A_2O_3 Samples

Sample Type	Thickness (cm)	Density (gm/cc)	30-40 GHz		55-60 GHz		90-100 GHz		130-140 GHz	
			k	$\tan \delta$ ($\times 10^{-3}$) (± 10)	k	$\tan \delta$ ($\times 10^{-3}$) (± 10)	k	$\tan \delta$ ($\times 10^{-3}$) (± 5)	k	$\tan \delta$ ($\times 10^{-3}$) (± 5)
Ampex 99.5%	3.0858	3.870	9.669 ± 0.008	31	9.662 ± 0.010	34	9.635 ± 0.005	38	9.633 ± 0.005	45
Ampex 99.9%	2.5425	3.907	9.755 ± 0.003	25	9.750 ± 0.005	32	9.750 ± 0.003	36	9.743 ± 0.003	42
Coors AD-995	3.8176	3.870	9.720 ± 0.008	29	9.712 ± 0.010	34	9.708 ± 0.005	38	9.702 ± 0.005	45
Coors AD-999	0.6368	3.882	9.71 ± 0.01	100 ± 40	9.71 ± 0.01	120 ± 40	9.71 ± 0.01	133 ± 20	9.71 ± 0.01	150 ± 20

C6795A/sn
13

4.3 Exploratory Alumina Formulations

In an effort to better understand the mechanisms controlling the dielectric loss in polycrystalline Al_2O_3 , and to uncover means for improving electrical and mechanical properties, several advanced formulations were fabricated and tested. Because of the exploratory nature of the investigation and in consideration of cost effectiveness, small samples were fabricated and characterized by cavity perturbation techniques. Two of these formulations were fabricated at ORNL and three at Rockwell International Science Center. The ORNL samples consisted of a fine-grained Al_2O_3 containing 0.2 w/o MgO and an Al_2O_3 composite with approximately 20 v/o fibrous SiC incorporated as a matrix. Both materials showed 30% - 50% improvement in fracture toughness over commercial polycrystalline Al_2O_3 . The samples fabricated and studied at Rockwell Science Center were made by initial calcining of Gibbsite powder (C331) at 700°C, followed by hot-pressing (HP) at 800°C to seal the sample in a Ni canister. Hot isostatic pressing (HIP) is then performed at 1300°C to fully consolidate the sample. TiO_2 is introduced at 2 m/o level to inhibit grain growth by addition of titanium isopropoxide in the powder preparation. Samples fabricated in this manner were of near-full density ($\rho = 3.9$), but showed high absorption at millimeter waves. Since C331 is known to contain alkali impurities, primarily sodium, subsequent samples were prepared with much purer Dispural powder, resulting in some improvement in loss characteristics. Finally, a high purity sample was prepared and hot isostatically pressed with no additives present. For this sample, the processing steps consisted of calcination at 700°C, isostatic pressing to form a green body, and then hot isostatic pressing at 1250°C. The resulting sample showed loss tangent values comparable to the best low loss commercial Al_2O_3 samples. However, the density achieved was only 3.5.

Results for the dielectric properties measured at room temperature and at 35 GHz for these exploratory samples are given in Table 3. Anomalously high values are obtained for the ORNL Al_2O_3 -SiC sample. They are most likely caused by the conducting nature of the SiC fibers, which, when imbedded in an



insulating dielectric matrix, creates a mixture with artificially high dielectric constants.

Table 3
Measured Room Temperature (23°C) Dielectric Properties of
Exploratory Al₂O₃ Materials at 35 GHz

Sample Composition	Dielectric Constant (±3%)	Loss Tangent
ORNL Samples		
1. Fine grain Al ₂ O ₃ (0.2 w/o MgO)	9.8	0.0009 ± 0.0002
2. Al ₂ O ₃ -SiC Composite (20 v/o SiC fiber)	20.6	0.21 ± 0.05
Rockwell Samples		
1. Hot isostatically pressed Al ₂ O ₃ (2 v/o TiO ₂)	9.7	0.0011 ± 0.0002
2. Hot isostatically pressed Al ₂ O ₃ (ultra-high purity starting powder and no additives)	7.8	0.0002 ± 0.0001

Other data indicated that the observed loss is qualitatively related to the level of additives in the samples. However, with high purity starting material and no sintering aids, full densification with calcination and hot isostatic pressing was not achieved. A much more in-depth materials development program appears to be necessary before the dielectric loss properties in polycrystalline ceramic Al₂O₃ can be improved over those achieved in selected commercial forms such as Coors AD-995, Wesgo AL-995, or the Ampex 99.5 and 99.9% Al₂O₃.

4.4 Zirconia-Toughened Alumina

Strengths in ceramics are governed by flaw types and their size distributions, and by the resistance of the material to crack extension. The addition of ZrO_2 as a second phase in an Al_2O_3 ceramic has been shown to dramatically improve the average strength properties. The chemically compatible ZrO_2 controls grain growth in Al_2O_3 , and thus minimizes localized stresses which can arise within and around large grains embedded in a finer grained matrix. The effect of surface cracks on strength degradation can also be minimized by the presence of ZrO_2 . The stress-induced phase transformation from tetragonal to monoclinic phase in ZrO_2 is accompanied by a molar volume increase (3%) which, in turn, places the surface under compressive stresses and increases the fracture toughness of the material. Consequently, the ZrO_2 - Al_2O_3 ceramic system offers the potential for achieving very high structural reliability, and flexural strengths three to four times higher than the average values (40 to 50 kpsi) for pure alumina have been achieved.

Such materials would be extremely attractive for gyrotron window applications, provided their millimeter-wave dielectric properties are not substantially degraded. To address this question, a series of samples were fabricated at both ORNL and Rockwell Science Center and characterized at 35 GHz to determine the magnitude of dielectric constant and loss tangent, and their dependences on ZrO_2 concentration. In addition to these custom samples, two partially stabilized commercial ZrO_2 samples (PSZ) were obtained from Nilcra Ceramics (USA) Inc., a TS and a MS grade. These are essentially pure ZrO_2 with 8 to 9 m/o MgO added to obtain a mixture of monoclinic, tetragonal and cubic phases. The flexural strength is somewhat higher for the MS grade material (109 Kpsi at room temperature by four-point bend tests for the MS grade, and 94 Kpsi for the TS grade), while the TS grade exhibits much better thermal shock resistance. It is hoped that these samples will have properties representative of 100% ceramic ZrO_2 in this study. The compositions of the ORNL samples were restricted to 20 v/o ZrO_2 , the primary purpose for this series being to study the dependence of materials properties on processing and



SC5357.4FR

on sintering aid concentration (Y_2O_3). Rockwell Science Center samples spanned the ZrO_2 concentration from 7.5 v/o to 60 v/o. Typical four-point bend test flexural strength for the 7.5 v/o formulation was approximately 75 kpsi, while the value for the 60 v/o formulation was 150 kpsi, or approximately three times that for pure alumina.

Room temperature dielectric properties for these samples at 35 GHz are given in Table 4. All measurements were performed on rod samples using the cavity perturbation technique. In addition, the PSZ materials were also characterized with the free-wave transmission and reflection method, using cube-shaped samples approximately 2 in. on each side. The data indicated that the addition of ZrO_2 substantially altered the dielectric properties of these materials from those for pure Al_2O_3 , and substantial increases in both the dielectric constant and the loss tangent values occurred with increasing ZrO_2 concentration. Consequently, the increase in millimeter-wave absorption in the as-fabricated materials offers no net advantage over the best pure commercial alumina. It must be emphasized that the fabrication process for these samples was not controlled to the extent that the materials parameters are exactly duplicated from sample to sample. Consequently, any general conclusions regarding systematic variations of dielectric properties with concentration need to take into account the possibilities that other parameters, such as impurity level, porosity, relative composition and phase assemblages, etc., may vary among the samples in this series.

Dielectric constant and loss tangent values are shown graphically in Figs. 2 and 3 as a function of ZrO_2 concentration. The data showed general trends of increasing dielectric properties with increasing ZrO_2 concentration. Previous cautions notwithstanding, these trends are almost certainly associated with composition effects.



SC5357.4FR

Table 4
Measured Room Temperature (23°C) Dielectric Properties of
Zirconia-Alumina Materials at 35 GHz

Sample Composition	Dielectric Constant (±3%)	Loss Tangent
<u>ORNL Samples</u>		
1. ALZRY 28-1 20 v/o ZrO ₂ •2 m/o Y ₂ O ₃	13.3	0.0032 ± 0.0005
2. ALZRY 19-4 20 v/o ZrO ₂ •2 m/o Y ₂ O ₃	12.4	0.0048 ± 0.0005
3. ALZRY 20-5 20 v/o ZrO ₂ •1 m/o Y ₂ O ₃	13.2	0.0037 ± 0.0005
4. ALZRY 27-3 20 v/o ZrO ₂ •1 m/o Y ₂ O ₃	12.5	0.0065 ± 0.0005
<u>Rockwell Samples</u>		
1. 7.5 v/o ZrO ₂ •2.5 m/o Y ₂ O ₃	11.5 11.6	0.0008 ± 0.0002 0.0011 ± 0.0002
2. 18.7 v/o ZrO ₂ •3 m/o Y ₂ O ₃	12.7	0.0025 ± 0.0005
3. 30 v/o ZrO ₂ •3 m/o Y ₂ O ₃	15.4	0.0053 ± 0.0005
4. 30 v/o ZrO ₂ •3 m/o Y ₂ O ₃	17.2	0.0120 ± 0.0020
5. 40 v/o ZrO ₂ •3 m/o Y ₂ O ₃	17.3	0.0085 ± 0.0015
6. 50 v/o ZrO ₂ •3 m/o Y ₂ O ₃	19.9	0.0125 ± 0.0025
7. 60 v/o ZrO ₂ •6.5 m/o Y ₂ O ₃	22.2	0.0090 ± 0.0020
<u>Nilcra Ceramics (USA) Inc. Samples</u>		
1. Partially Stabilized ZrO ₂ , TS	28.5	0.0022 ± 0.0002
2. Partially Stabilized ZrO ₂ , MS	27.2	0.0033 ± 0.0002

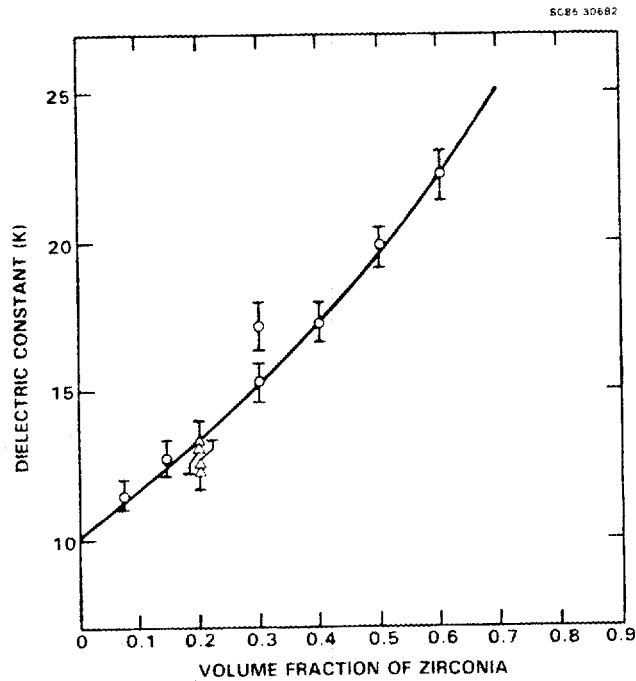


Fig. 2 Measured room temperature dielectric constant values at 35 GHz for $ZrO_2-Al_2O_3$ samples as a function of ZrO_2 concentration.

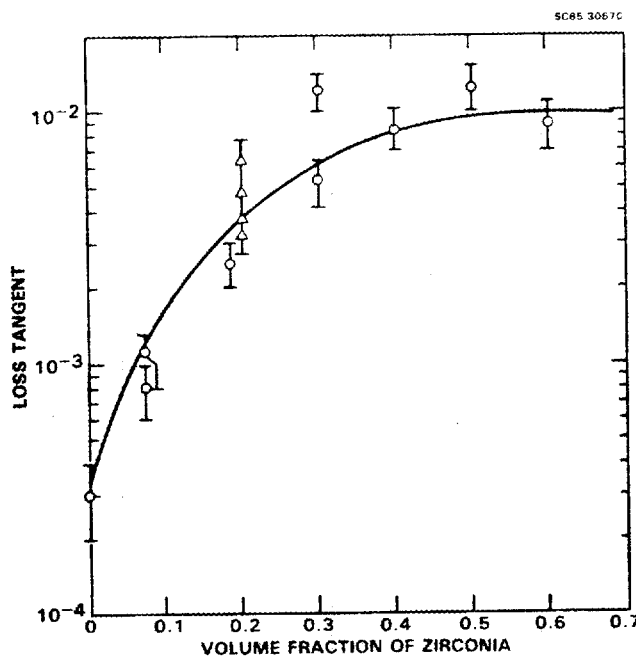


Fig. 3 Measured room temperature loss tangent values at 35 GHz for $ZrO_2-Al_2O_3$ samples as a function of ZrO_2 concentration.



SC5357.4FR

Although it is probable that loss tangents can be lowered by further materials research, the observed increase in dielectric constant with ZrO_2 concentration places certain inherent restrictions on potential window applications in this class of material. Since the electrical pathlength within a material is proportional to the square root of the dielectric constant, a very high value implies larger interface reflections which need to be cancelled in resonant conditions with smaller physical pathlengths. Consequently, absolute dimensional tolerances become more stringent and, in extreme cases, the window thicknesses required for a given bandwidth become so small as to be impractical from a structural viewpoint. Consequently, using materials with ZrO_2 concentration in excess of 10-15 v/o probably is not feasible, although the greatest strength and fracture toughness are obtained in the 60-70 v/o range. Even at these low concentrations, significant improvements in strength properties (30-50%) can still be achieved. Loss tangents observed in the existing materials for this concentration range are excessively high, and the basic question remains whether this excess loss is associated primarily with intrinsic properties of mixed composition ceramic systems, or whether it can be minimized by control of impurities, microstructure and stoichiometry.

4.5 Low-Loss Fluids

The dielectric properties of a series of low-loss candidate cooling fluids were determined at 8.4 and 35 GHz for temperatures up to 125°C. These fluids were chosen as alternatives to the fluorocarbon fluids in gyrotron window cooling applications, based on their higher flash temperature and lower potential health hazard. They were supplied by TRW and consisted of two petroleum hydrocarbon oils and two alkanes. The diala oil and transcresol oil are essentially identical in chemical composition and are mainly naphthenes. The n-dodecane and tetradecane are known to have very low millimeter-wave absorption.⁷

The measurements were performed by resonant cavity techniques using carbon tetrachloride as a reference standard. Measurements were made at

SC5357.4FR

8.4 GHz at room temperature and at 35 GHz over the range 25-125°C. In addition, comparison studies were also carried out at 8.4 GHz to determine the effect of water contamination on the dielectric properties of the fluids. The data obtained are summarized in Tables 5 and 6. The dielectric properties were found to be independent of frequency over the range studied, with the alkanes showing significantly less absorption than the petroleum oils. Of the four materials studied, tetradecane has the lowest loss tangent (0.003 to 0.004), with the oils exhibiting losses approximately an order of magnitude higher. The presence of water in the samples at the 100-200 ppm levels causes a slight change in the dielectric constant ($\sim 0.03\%$), as well as an increase in the loss tangent (3 to 6×10^{-4}). This increase is negligible compared to the loss tangent values for the petroleum oils, but it is significant in the very low-loss alkanes. The dielectric constants were found to decrease linearly with increasing temperature. As shown in Fig. 4, the rate of change is almost identical for the three cases studied and most likely is due to thermal expansion in the fluids. The loss tangents remained constant over the temperature range studied for the alkanes, but increased significantly in transcrest oil.

It can be concluded from the data that the alkanes are superior both to the petroleum oils studied in this effort, and to the fluorocarbon fluids studied previously in terms of loss characteristics in the millimeter-wave region. The loss tangent generally decreases, and the flash temperature increases with increasing molecular weight in the alkane series. This is offset by the fact that the viscosity increases with molecular weight, so that a tradeoff study needs to be performed to arrive at the optimal choice of fluid for specific coolant applications.

Dielectric properties of normal alkanes in the microwave and far-IR regions have been studied by Stumper⁷ as a function of frequency and temperature. The absorption observed in the far-IR has been attributed either to a reorientational relaxation process of weak permanent dipoles attached to the ends of the molecules, or to transient dipoles induced in the nonpolar molecules by localized electric fields. The absorption bands for these liquids



SC5357.4FR

Table 5
Measured Room Temperature (23°C) Dielectric
Properties of Low-Loss Fluids at 8.4 GHz

Material	k (± 0.005)	tan δ (± 0.0002)
n-dodecane (71 ppm H ₂ O)	2.004	0.0007
n-dodecane (163 ppm H ₂ O)	2.009	0.0010
Tetradecane (Aldrich, 99%)	2.028	0.0004
Diala oil (77 ppm H ₂ O)	2.214	0.0020
Diala oil (165 ppm H ₂ O)	2.221	0.0026
Transcrest oil (dried)	2.218	0.0023
Transcrest oil (undried)	2.220	0.0025

Table 6
Measured Dielectric Properties of Low-Loss Fluids
at 35 GHz as Function of Temperature

	25°C	75°C	125°C
<u>Transcrest Oil (Dried)</u>			
k (± 0.01)	2.220	2.152	2.083
tan δ (± 0.0005)	0.0022	0.0036	0.0047
<u>n-dodecane (71 ppm H₂O)</u>			
k (± 0.01)	2.003	1.952	1.875
tan δ (± 0.0002)	0.0006	0.0006	0.0005
<u>Tetradecane (Aldrich, 99%)</u>			
k (± 0.01)	2.024	1.974	1.917
tan δ (± 0.0001)	0.0003	0.0003	0.0003

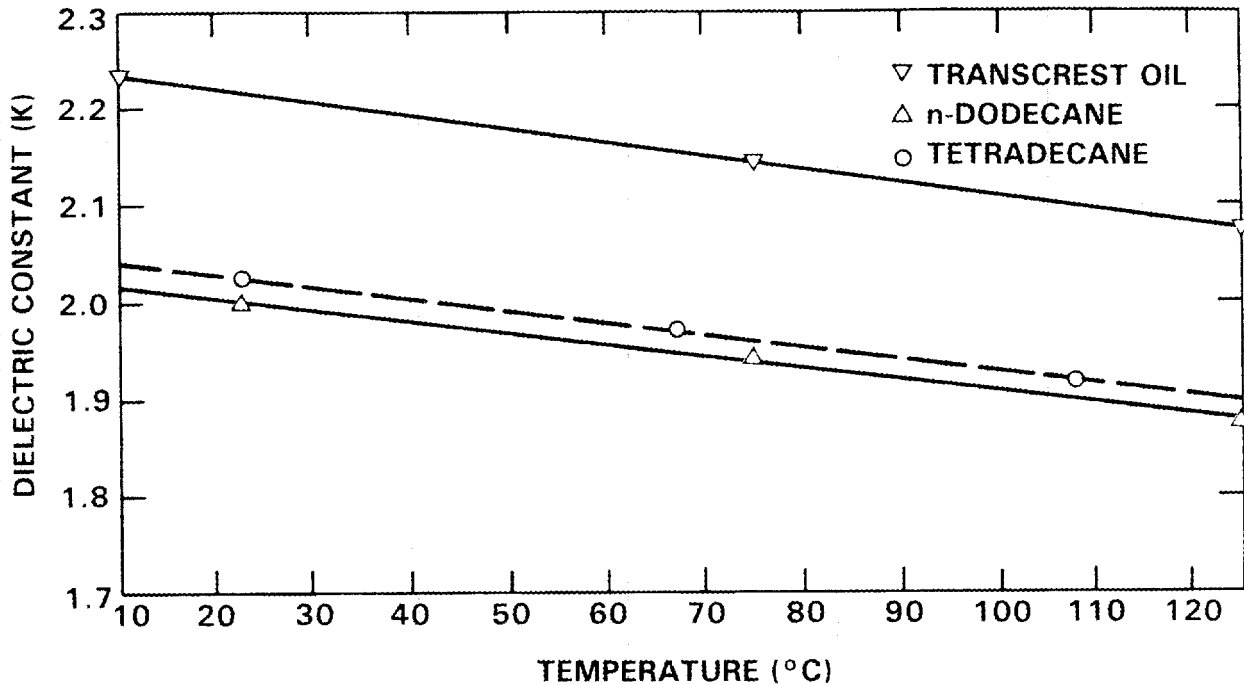


Fig. 4 Measured dielectric constant values for low-loss fluids as a function of temperature.

typically peak between 2000 and 5000 GHz, with their low frequency wings in the millimeter-wave region decreasing with increasing molecular weight. The general trends in the density, viscosity and millimeter-wave absorption properties for the alkanes are illustrated in Table 7. Clearly, fluid flow properties need to be considered in addition to millimeter-wave loss properties in cooling applications. It is also worth noting that the room temperature dielectric properties obtained for n-dodecane at 30-40 GHz by Stumper are in good agreement with the results of the current study.

4.6 Chemical and Microstructural Analysis

The preliminary study initiated in the previous year's effort and described in ORNL/SUB/83-51926/1 (Rockwell Report SC5337.2TR) was continued in the current program. This study was aimed at identifying the materials properties giving rise to differences in observed millimeter-wave absorption for



Table 7

Room Temperature (20°C) Dielectric Loss at 100 GHz and Viscosity
Data for Normal Alkanes as Obtained from Literature*

n-alkanes	Density (gm/cc)	Viscosity (cp)	Loss Tangent (X10 ⁻⁴)
Pentane (C ₅ H ₁₂)	0.626	0.240	12
Hexane (C ₆ H ₁₄)	0.659	0.326	10
Heptane (C ₇ H ₁₆)	0.684	0.409	8
Nonane (C ₉ H ₂₀)	0.718	0.711	7
n-decane (C ₁₀ H ₂₂)	0.730	0.92	5.5
n-dodecane (C ₁₂ H ₂₆)	0.749	1.35 (25°C)	4.5
n-hexadecane (C ₁₆ H ₃₄)	0.773	3.34	4.0

* Loss tangent values are from V. Stumper, Advances in Molecular Relaxation Processes 7, 185-208 (1975). Density and viscosity values are from CRC Handbook of Chemistry and Physics, Chemical Rubber Co., Cleveland, OH.

polycrystalline alumina. In the previous effort, average grain size and size distribution, chemical composition, crystalline phases, and intergranular properties of select Al₂O₃ samples were determined by a combination of SEM, x-ray diffraction, STEM and energy dispersive x-ray analysis. The sample chosen for study consisted of two Al₂O₃ types which exhibited low loss (Coors AD-995 and Wesgo Al-995) and two which exhibited significantly higher loss (Coors AD-999 and Union Carbide/ORNL hot-pressed Al₂O₃). In the current effort, analysis of these samples was performed in much greater detail, and it was extended to a number of new samples.

In summary, the average grain size of the better materials was found to be substantially larger (50-30 μm in comparison to 0.5-5 μm). Direct evidence was found for the deterioration of properties in the Union Carbide material due to the presence of contaminants from the hot pressing process; specifically, sodium, silicon, chlorine, potassium and calcium. The x-ray analysis of the Union Carbide hot-pressed sample in the SEM showed significant differences in trace element composition at the sample interiors away from the



SC5357.4FR

contamination introduced at the surfaces from the hot pressing procedure. This gradient correlated directly with the observed variation of loss properties within the sample. Large-scale porosity was also apparent in the materials with relatively low losses, as were calcium-alumino silicate glassy phases at the grain junction. The concentration of secondary crystalline phases such as quartz, calcium aluminate and spinel varied significantly from the high of all three in the Wesgo Al-995 to reduced concentration in the Coors AD-995, and complete absence of some in the samples showing the higher losses. Since pure secondary phases in general are not very absorbing, their contributions to the total loss are not expected to be significant at the typical concentrations found in these materials (<1%). Consequently, it can be concluded that the presence and distribution of additional impurities within these and the primary Al_2O_3 grains are controlling the loss properties.

The systematic analysis of the microstructures of the materials using analytical electron microscopy was carried out with a comparison of two of the materials already examined: Coors AD-995, which had low-loss properties, and Union Carbide hot-pressed Al_2O_3 , which did not. Another material, Ampex 995, which had virtually identical loss tangent values to the Coors AD-995, was also examined.

The Ampex 995 and Coors AD-995 samples have completely different topographies in contrast to the fact that their dielectric properties are very similar. The Coors sample is characterized by fairly large grains of essentially pure $\alpha\text{-Al}_2\text{O}_3$, with the impurities concentrated at the grain boundaries and the grain junctions. An example of this microstructure is shown in Fig. 5, where pockets of glass are found as triangular-shaped regions. These glasses vary in composition, but consist principally of a mixture of SiO_2 and CaO with the Al_2O_3 ($\text{SiO}_2\cdot\text{CaO}$). The glass pocket in Fig. 6, for example, has a composition $3\text{Al}_2\text{O}_3\cdot 6(\text{SiO}_2\cdot\text{CaO})\cdot\text{Na}_2\text{O}$ and extends along the grain boundaries. The glass phases do not always contain SiO_2 , and the soda concentrations also vary widely. The grain boundaries seem to contain mostly Ca as an impurity and, indeed, many of the boundaries are free from impurities to the limit of



Fig. 5 Glassy triple points in Coors-AD-995 alumina.

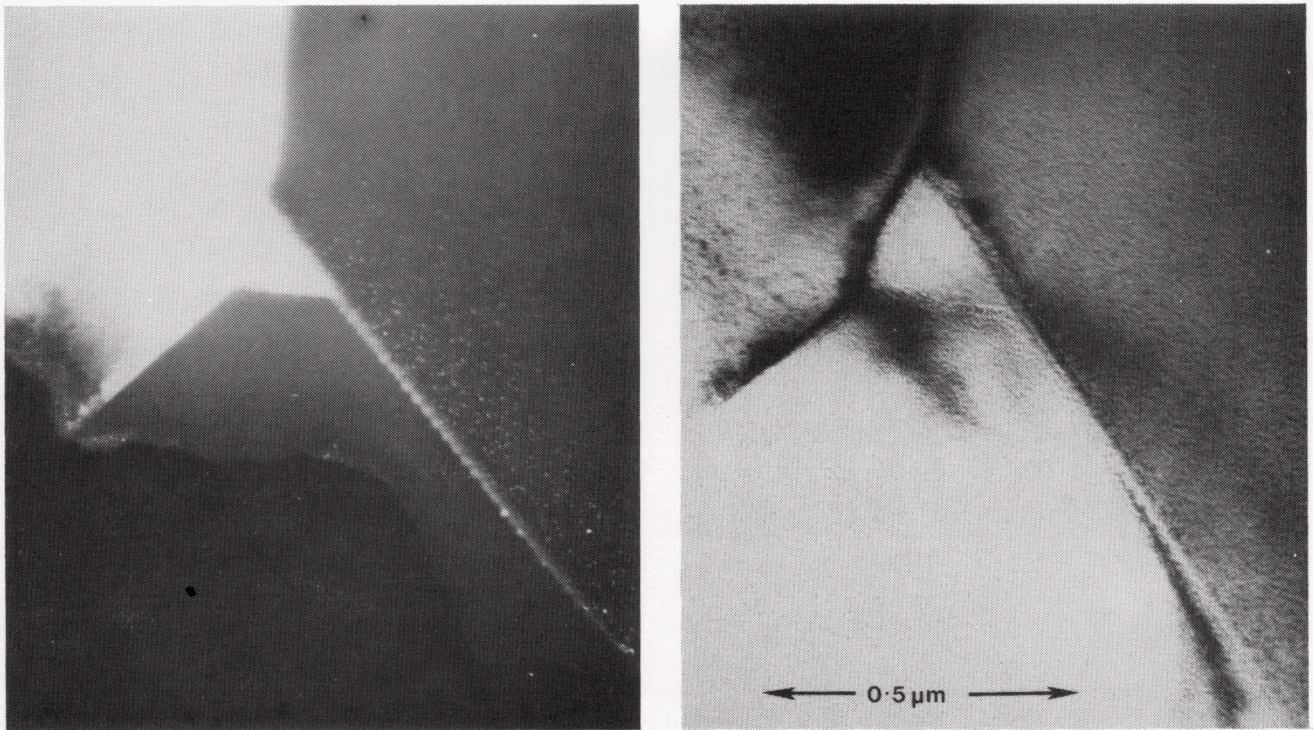


Fig. 6 Bright field, dark field pair of a glassy triple point and surrounding grain boundaries in Coors AD-995.

SC5357.4FR

Fig. 6, but clearly the boundary phases are a sink for most of the impurities. The only element detected in the grains themselves, other than Al and oxygen, is sulphur, which maintains a concentration in the hundreds of parts per million range in some grains and glassy pockets alike.

On the other hand, the Ampex 995 ceramic shows almost no evidence of a glassy phase at the boundaries (Fig. 7), although an analysis of the grain boundaries and junctions shows that Ca does, in fact, segregate there. The concentrations often reach 1% or more of the volume of Al_2O_3 analyzed, which always contains material adjacent to the boundary. Similarly, fractional percentage concentrations of sulphur and Sn can often be detected at grain junctions, and are often found to be depleted at the grain boundaries in comparison to the grains themselves. The sulphur concentrations at the grain junctions are notably higher than the concentrations in the grains themselves, which never exceed the hundreds of parts per million range and are often undetectable.

The Union Carbide hot-pressed sample, which in contrast has much poorer loss properties, is littered with small voids. They vary between 1000 and 10,000Å in diameter and are often faceted (Fig. 8). There is no evidence for porosity at the grain junctions (Fig. 9), and careful examination of these triangular regions shows them not to be glassy, but instead to exhibit diffraction contrast from the surrounding grains (Fig. 10). There is little evidence for segregation of impurities to either the grain boundaries or junctions, but some of the grains themselves show Ce and Ca concentrations in the range of 0.1 atomic% and potassium concentrations an order of magnitude lower. There are exceptionally high concentrations of sulphur in the grains, as high as 2 atomic% in some cases, which is three orders or magnitude larger than in either the Coors AD-995 or Ampex 995. There were also concentrations of several atomic% of Sc in some grains which, along with potassium, was common only to this material.

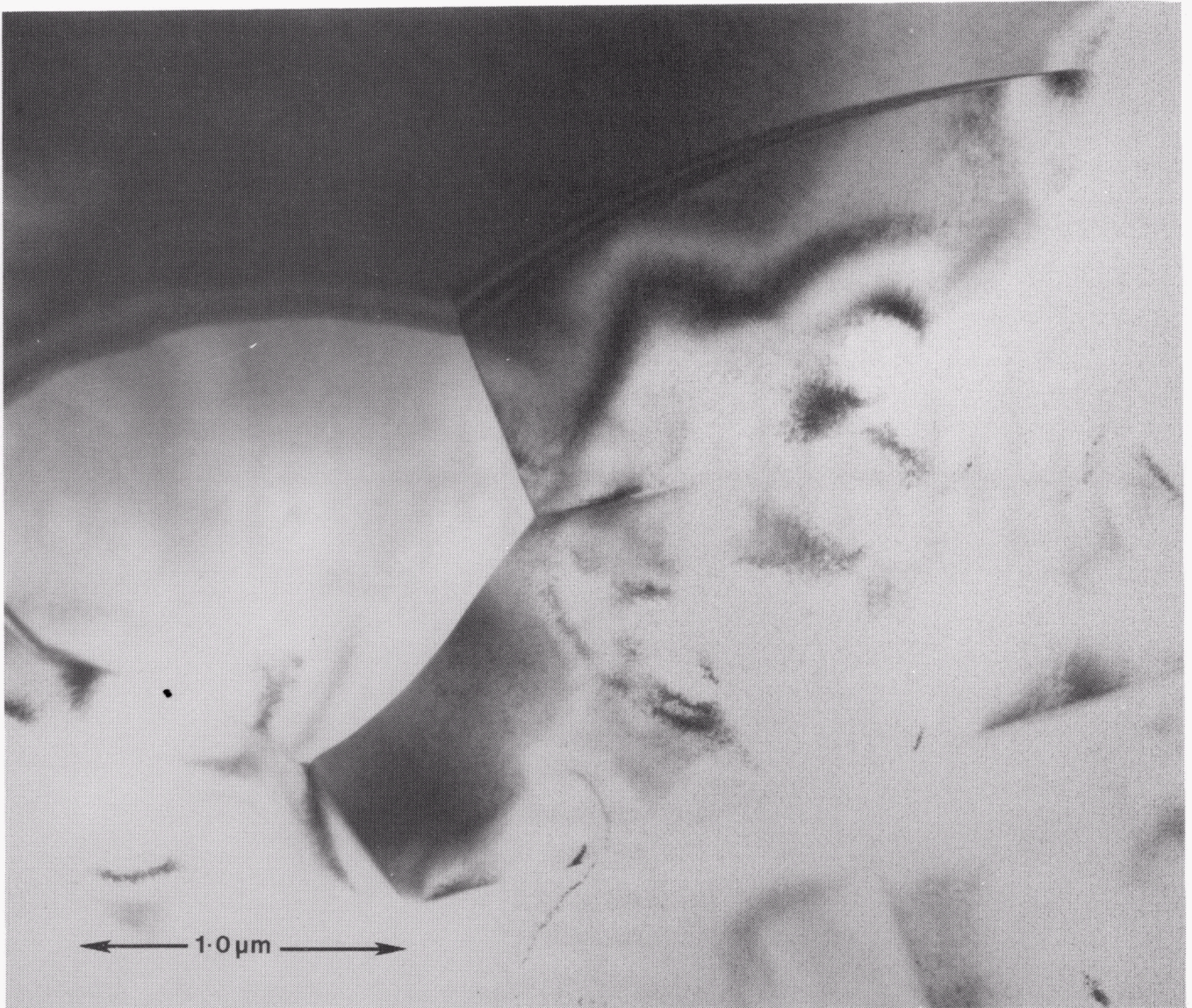


Fig. 7 Bright field micrograph of the microstructure of Ampex 995 showing the absence of any boundary phase.

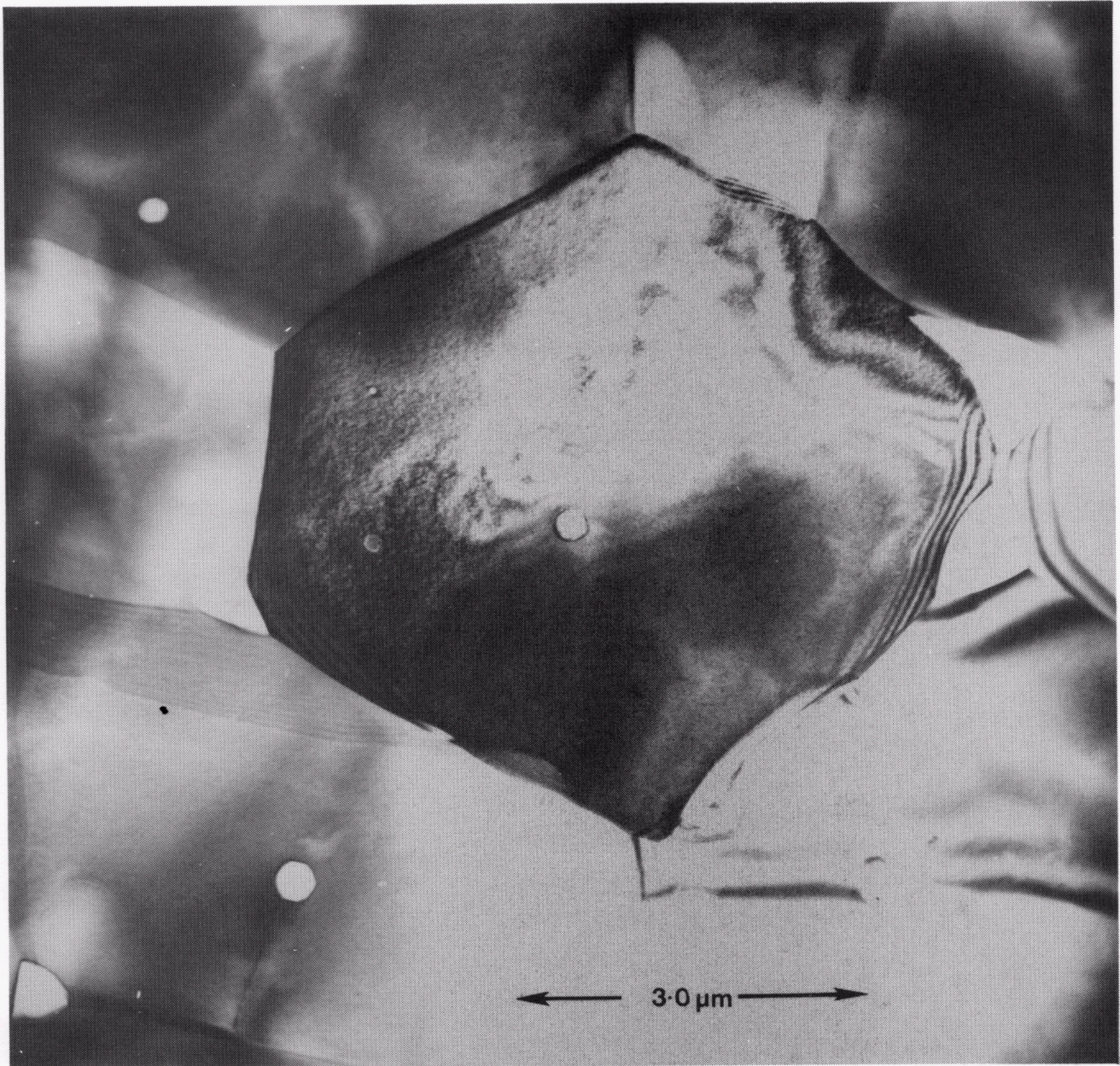


Fig. 8 Bright field micrograph of the microstructure of the Union Carbide hot-pressed Al₂O₃ showing the presence of small voids.

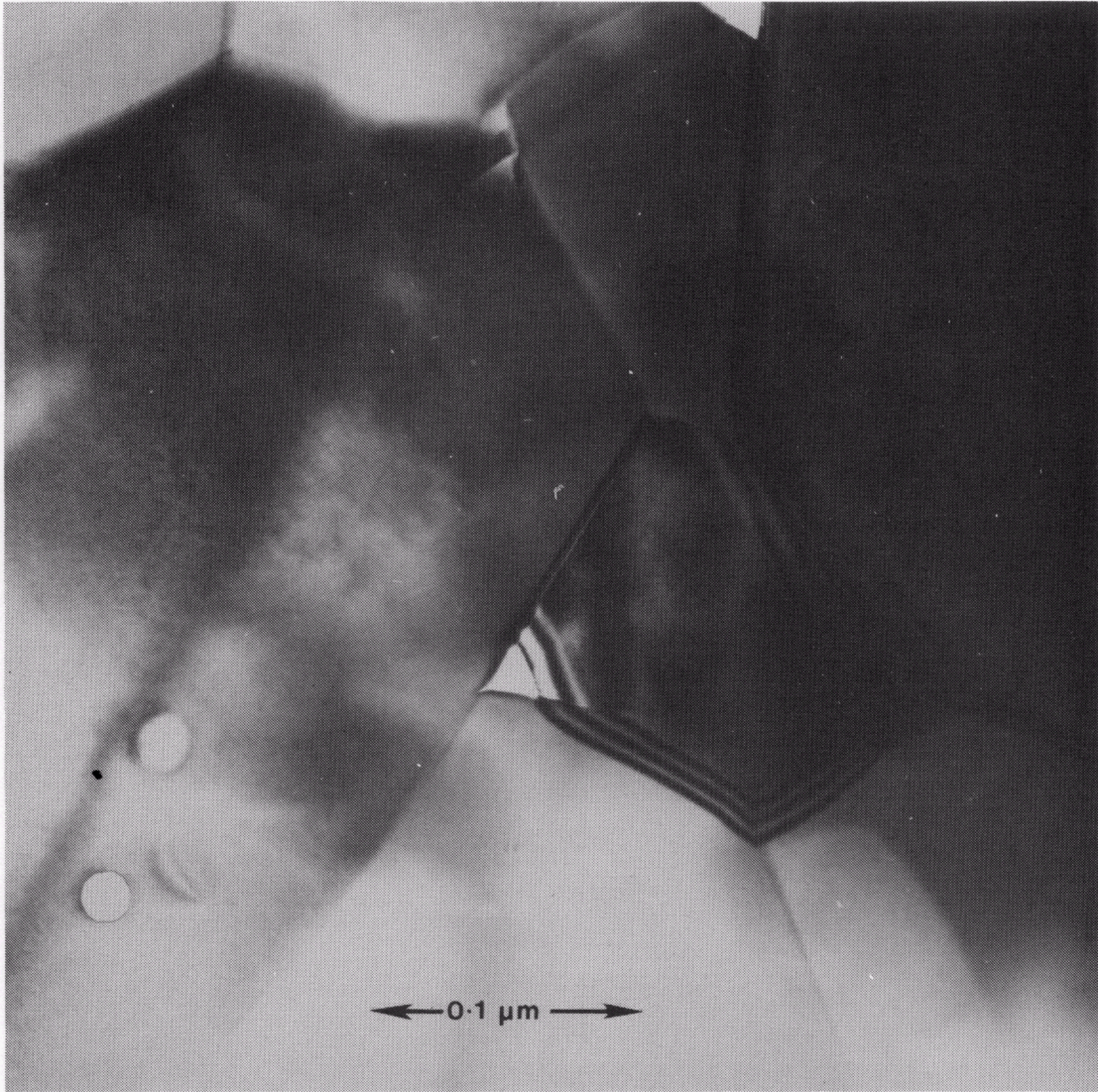


Fig. 9 Bright field micrograph from the Union Carbide Al₂O₃ showing the triangular holes at the grain corners.

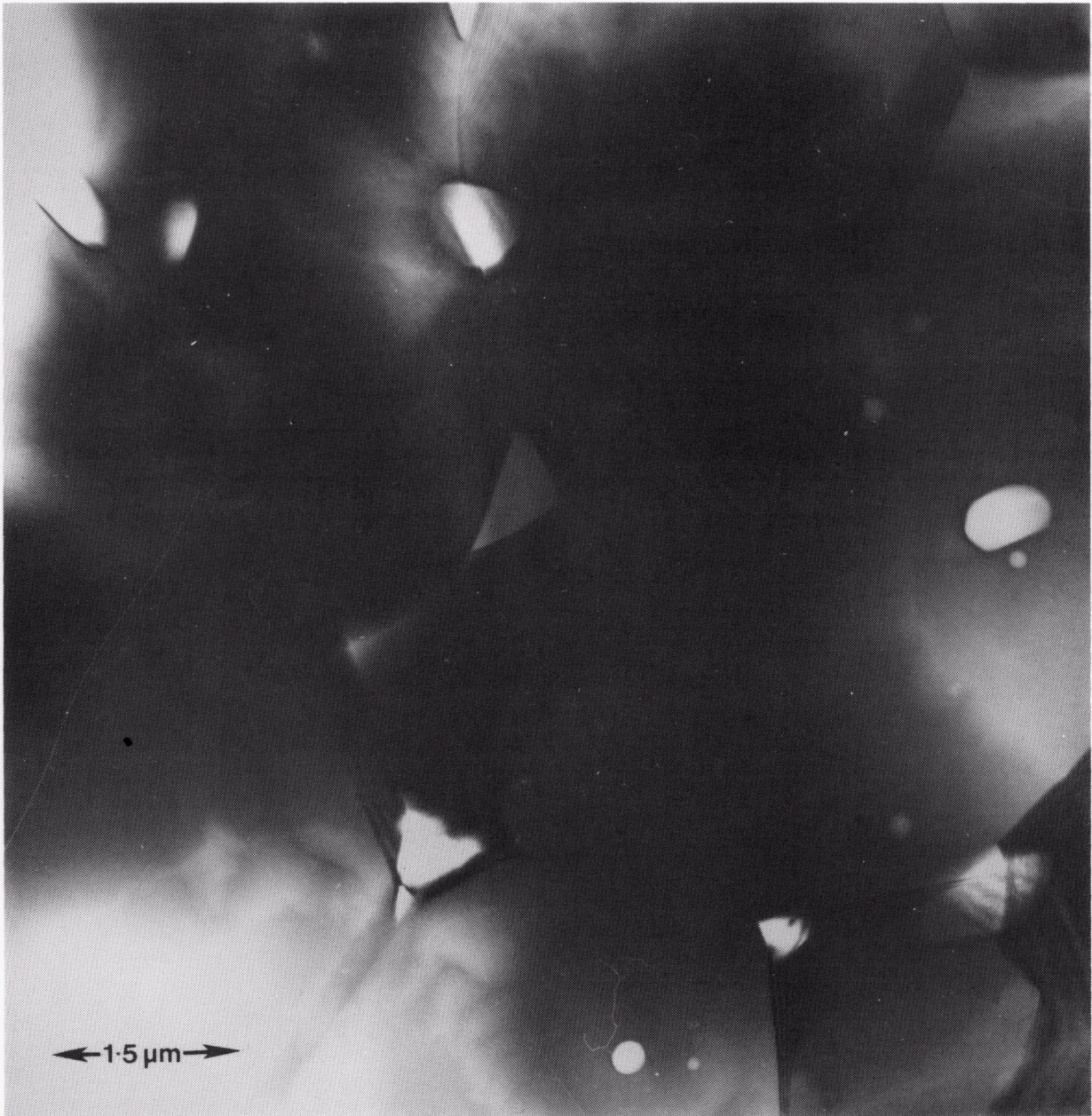


Fig. 10 Bright field micrograph from the Union Carbide Al₂O₃ showing the faint diffraction contrast from the grain junction.

SC5357.4FR

From these results, the consistency between the materials with lower loss tangent values would seem to be the absence of fine porosity (which in the case of Coors AD-995 is replaced by large voids at the grain boundaries of the order of several microns) and the presence of only very low concentrations of impurities within the grains themselves. Pure secondary phases by themselves apparently do not contribute to any significant increase in loss, but their presence in high concentrations undoubtedly will lead to higher levels of intragranular and grain boundary impurities, which can cause excessive millimeter-wave absorption.

Because of the large grain surface-to-volume ratios in fine grain materials, additives and impurities need to be controlled to much lower concentration levels to achieve the same loss properties as larger grained materials. However, such low levels of additive may not be compatible with full densification of the ceramic during processing, as illustrated by the difficulties encountered in producing fully dense samples using ultra-pure starting powder and no sintering aids.

Materials analysis was also carried out on select samples of the exploratory Al_2O_3 formulations and $\text{ZrO}_2\text{-Al}_2\text{O}_3$ samples. The results obtained are consistent with the above general observations. The grain structures for the Rockwell ultra-high purity hot isostatically pressed Al_2O_3 sample and the ORNL fine-grain Al_2O_3 sample are shown in Fig. 11a and 11b, respectively. Full densification was not achieved with the Rockwell sample, but excellent loss characteristics were obtained, which most probably is due to the observed low concentrations of intragranular impurities. The ORNL sample is nearly fully dense, but exhibited higher loss, together with many small voids. In fact, the loss tangent values for this sample were found to be significantly higher than the much larger-grained commercial samples such as Coors AD-995, even though the overall detected impurity levels were much less.

Figure 12a shows the microstructure of the near fully dense Rockwell hot isostatically pressed sample. The distribution of Ti within the sample resulting from the added TiO_2 for achieving densification is shown in Fig.

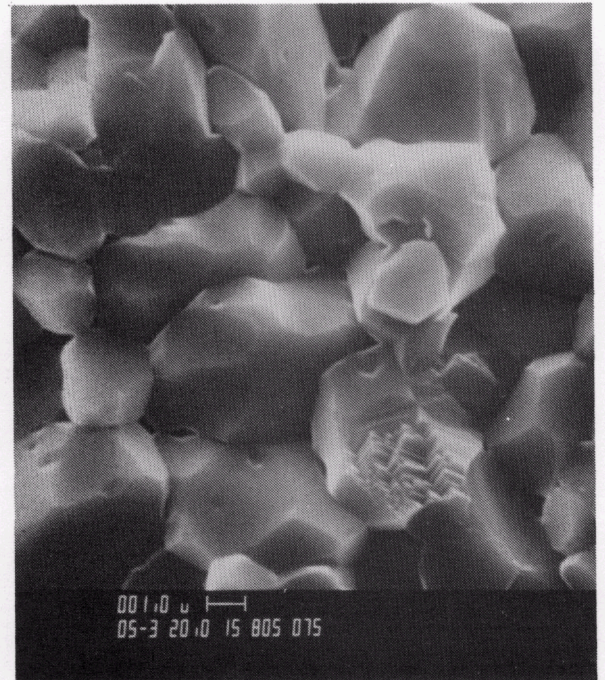
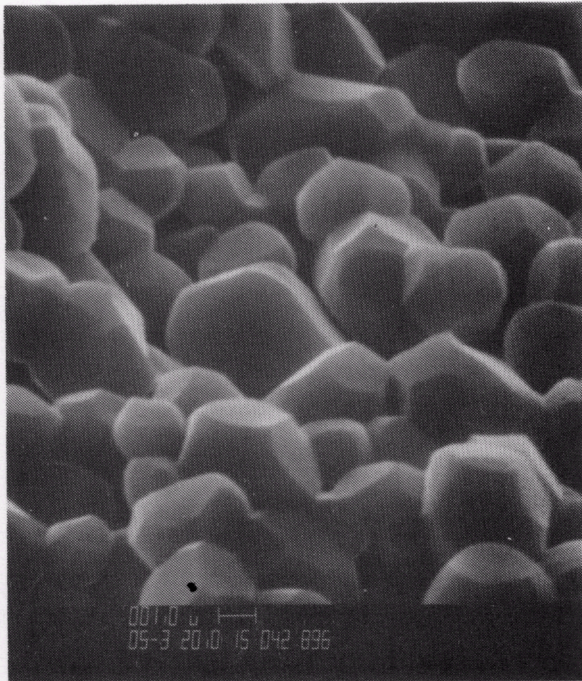


Fig. 11 (a) SEM of ultra-high Al_2O_3 sample fabricated at the Science Center by hot isostatic pressing; (b) SEM of ORNL fine grain Al_2O_3 sample.

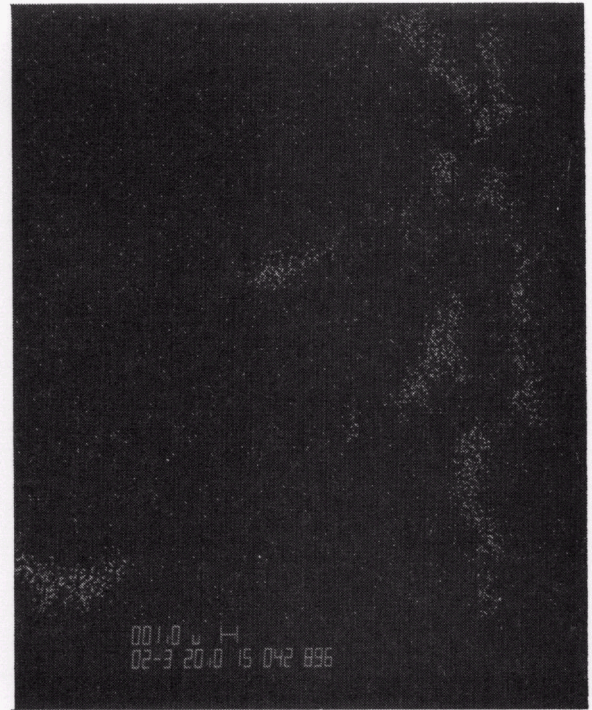
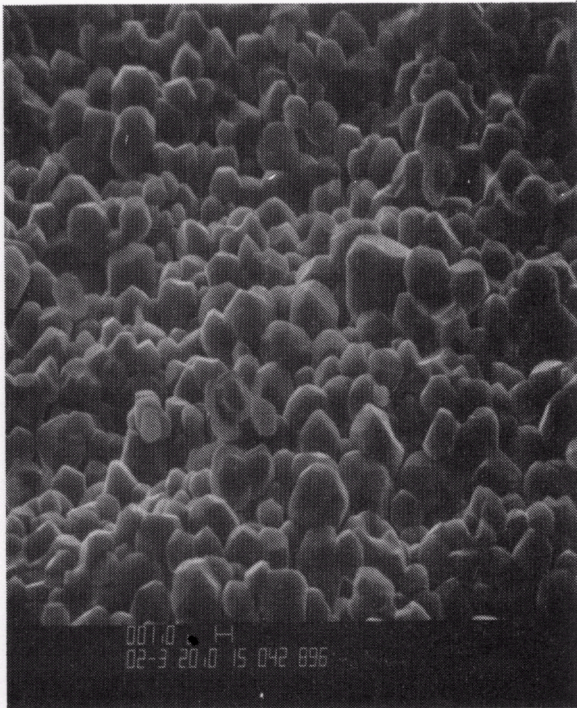


Fig. 12 (a) SEM of hot isostatically pressed Al_2O_3 sample containing TiO_2 as densification aid fabricated at the Science Center; (b) elemental x-ray mapping by EDAX showing distribution of Ti within sample illustrated by (a)

SC5357.4FR

12b, obtained by elemental x-ray mapping with EDAX. Ti was found to occur as a secondary oxide crystalline phase occurring at the grain boundary, as well as incorporated within individual grains. As expected, this sample showed high dielectric loss. These results are good illustrations of the previously stated sensitivity of dielectric loss properties in fine-grained A_2O_3 to trace additives.

Chemical and microstructural analyses were also carried out on the ORNL series of $ZrO_2-A_2O_3$ samples (ALZRY 28-1, 19-4, 20-5 and 27-3). These samples showed a variation in dielectric constant between 12.4 and 13.3, and loss tangents between 0.0032 and 0.0065. XRD indicated that the primary crystalline phases in these samples are $\alpha-A_2O_3$, tetragonal, monoclinic and cubic ZrO_2 , $Y_{0.15}Zr_{0.85}O_{1.93}$ and SiO_2 . $\beta-A_2O_3$ was detected in sample ALZRY 27-3, which is probably the cause for the higher loss tangent value observed in this sample (0.0065). Of the remaining three samples, ALZRY 19-4 showed the highest loss. Chemical analysis by EDAX performed on a fractured surface revealed relatively high concentrations of Fe, Na, Ca, Cl and potassium (Fig. 13). The

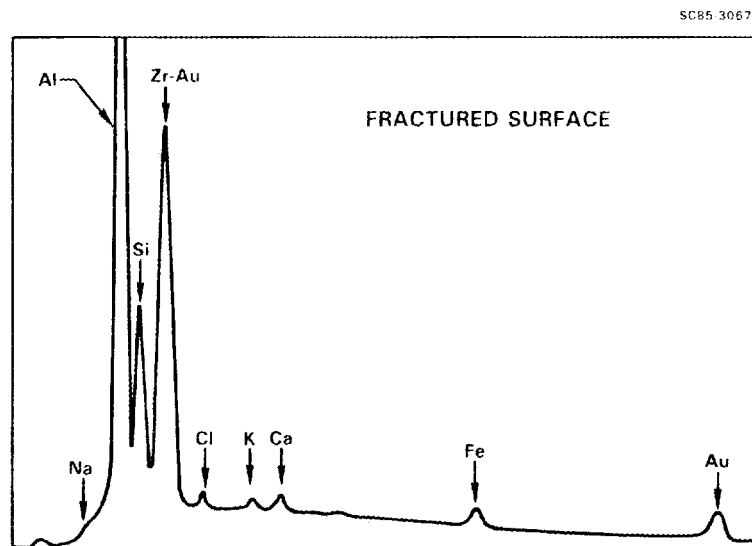


Fig. 13 Microprobe chemical analysis by EDAX of fractured surface for ORNL $ZrO_2-A_2O_3$ sample ALZRY 19-4.

Fe was found to occur as intergranular inclusions and to be distributed on the surface and within the grains. Typical distribution of Fe in this sample is shown in Fig. 14.

The distribution of ZrO_2 grains within the Al_2O_3 matrix for samples ALZRY 19-4, 20-5 and 28-1 are shown in Figs. 15, 16a and 16b, respectively. The contrast between the white ZrO_2 grain and the darker Al_2O_3 is obtained by backscattered electron imaging on the SEM. The ZrO_2 grains occur at the grain boundaries and triple points, and are embedded inside the Al_2O_3 grains. Typical ZrO_2 grain sizes are about $0.5 \mu m$. Since even trace contamination occurring within the Al_2O_3 grains have been demonstrated to lead to high absorption, it is not surprising that these samples show the level of loss that they do. Indeed, as the concentration of ZrO_2 in the sample is increased, one would qualitatively expect the loss first to increase, and then to decrease as the material approaches pure ZrO_2 . This is consistent with the general trend of the data shown in Fig. 3, keeping in mind that the loss tangent values obtained for PSZ samples are in the range 0.002-0.003.

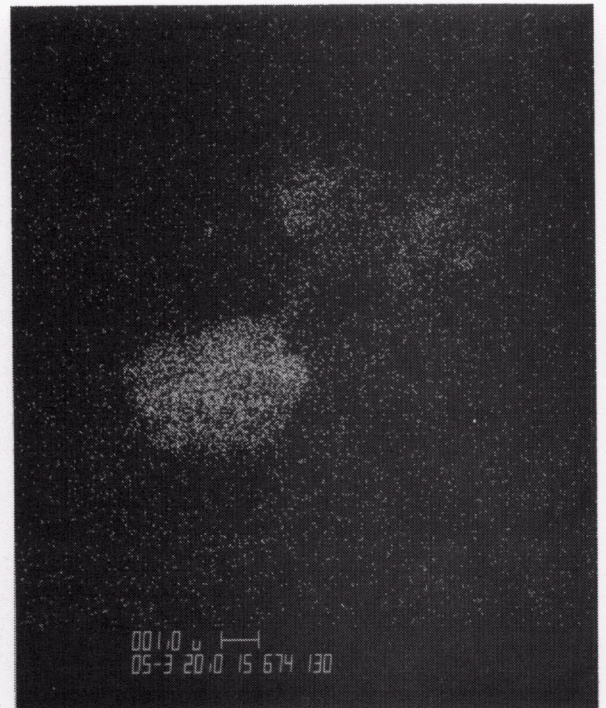
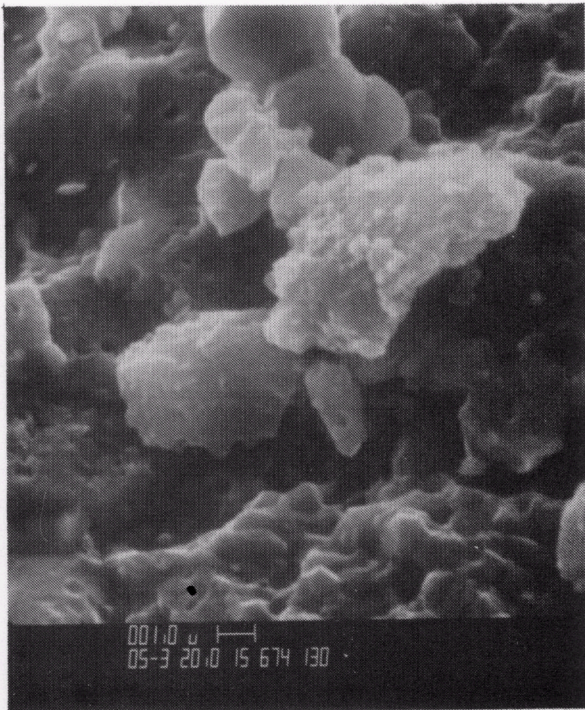


Fig. 14 (a) SEM of fractured surface of ORNL $ZrO_2-Al_2O_3$ sample ALZRY 19-4 showing inclusions; (b) elemental x-ray mapping by EDAX showing distribution of Fe within sample illustrated in (a).

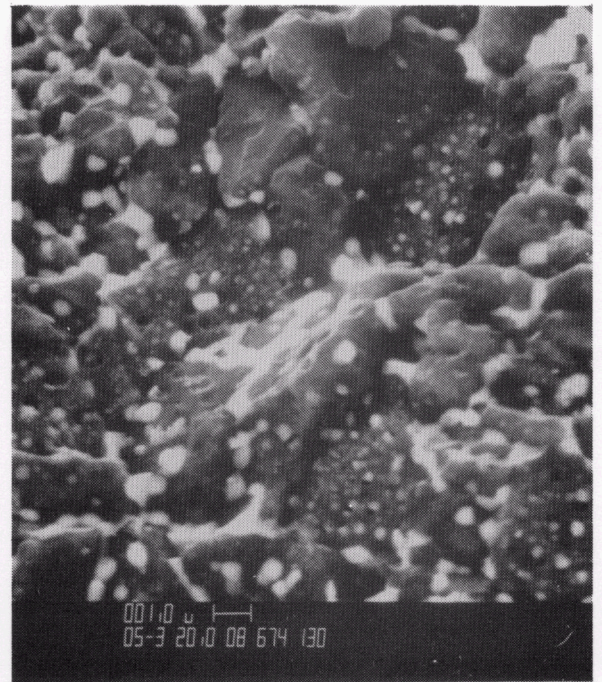


Fig. 15 SEM showing the distribution of ZrO_2 (white) in Al_2O_3 matrix for ORNL sample ALZRY 19-4.

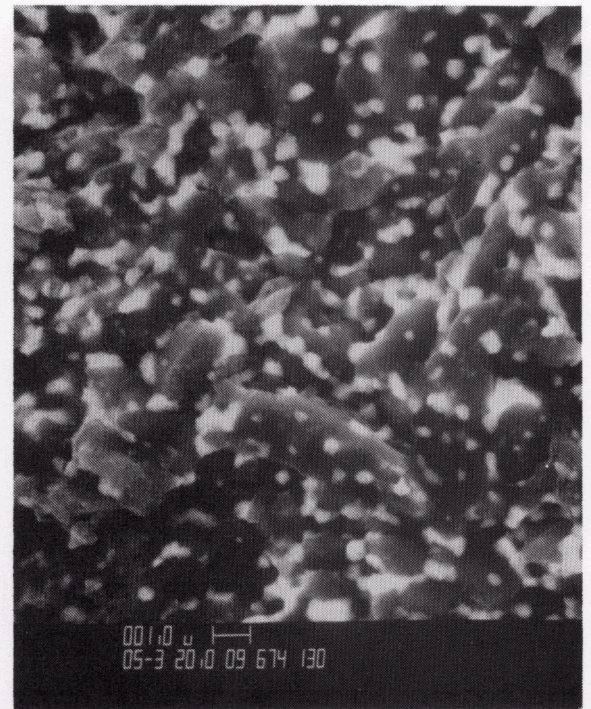


Fig. 16 (a) SEM showing the distribution of ZrO_2 (white) in Al_2O_3 matrix for ORNL sample ALZRY 20-5; (b) SEM showing the distribution of ZrO_2 (white) in Al_2O_3 matrix for ORNL sample ALZRY 28-1.

5.0 CONCLUSIONS AND RECOMMENDATIONS

The measurement results obtained for single crystal sapphire over the frequency range 30-140 GHz indicated that the dielectric constants along the principal axes are virtually independent of frequency. Their loss tangents are significantly lower than any ceramic material studied in this program, and are less than 10^{-4} at frequencies below 60 GHz and between $1-2 \times 10^{-4}$ over the frequency range 90-140 GHz. These values were found to be independent of the quality of the crystal samples studied, implying that variations in air bubble content and crystal defects for high optical quality materials are not significant in terms of millimeter-wave dielectric properties.

The commercial alumina samples all showed a more gradual fall-off in loss tangent values with decreasing frequency when compared to sapphire, and have magnitudes two to three times higher in the 90-140 GHz range for the best materials. The lowest loss commercial materials studied to date are the Coors AD-995, Ampex 99.5% and Ampex 99.9% alumina, where loss tangents between $3-5 \times 10^{-4}$ are observed between 30-140 GHz.

Comparison of the results obtained in the current study with those obtained by Afsar and Button on similar materials indicated that good agreements are obtained for the Coors AD-999 and Wesgo Al-995 alumina. However, a substantial difference is observed for single crystal sapphire, with the current results being a factor of two to three times lower in the frequency range 100-140 GHz. This difference is due possibly to polarization effects which may be present, but not accounted for, in the previous study by Afsar and Button.

Since the low dielectric loss in sapphire has made it a primary candidate for high power gyrotron window applications, this discrepancy must be resolved, and a set of reliable data must be established over the millimeter-wave region of interest for this material. It is recommended that a coordinated experimental effort be undertaken with independent investigators using various measurement techniques on identical controlled samples to produce a set of self-consistent data of known absolute accuracy.



In principle, the observed loss in single crystal sapphire can be reduced substantially by operating at low (cryogenic) temperatures. Experimental data in the millimeter frequency region below room temperature are not currently available in the literature. However, preliminary data taken on a sample of sapphire (Crystal System Hemex) and a sample of alumina (Coors AD-995) at liquid nitrogen temperatures are very encouraging. A reduction in loss of approximately 25% was observed in the ceramic material, while the loss tangent in sapphire decreased to below 5×10^{-5} at 100 GHz, which is the limit in measurement sensitivity with the existing instrumentation on the sizes of samples used. These observations are consistent with the assumption that the intrinsic loss in sapphire is very temperature-dependent, while the excess extrinsic loss in ceramic alumina is not. If these observations are verified, then only a marginal improvement is expected in alumina, but a very substantial improvement can be expected in single crystal sapphire. With the anticipated low loss at cryogenic temperature for sapphire, measurements methods need to be improved to provide the necessary sensitivity. In view of the potential advantages which can be attained with low temperature operations for sapphire in window applications, it is recommended that an experimental program be undertaken to determine the dielectric properties of this material at temperatures down to liquid nitrogen temperature. Concurrently an engineering development program needs to be initiated to address the issues associated with the design of cooled gyrotron windows.

The exploratory materials development effort for improving the dielectric and strength properties of ceramic alumina proved to be extremely valuable in terms of understanding the loss mechanisms in ceramics at millimeter waves. While the effort did not produce materials with simultaneously optimized strength and millimeter-wave loss properties, basic insights that can potentially lead to new methodologies and fabrication approaches for advanced materials development were obtained. The combination of dielectric and microstructural characterization studies have indicated that intragranular impurity is one of the dominant causes of high millimeter-wave absorption, and is most likely to occur in fine-grained alumina and in materials with high initial concentrations of additives and contaminations.

SC5357.4FR

To achieve high strength and low loss, fabrication methods which can result in fully dense fine-grained alumina with very low impurities must be developed. In practice, this is difficult to accomplish, since the traditional way for obtaining high density and for controlling excessive grain growth is through additions of sintering aids and chemically compatible second phases. This is often not consistent with the latter requirement of low intragranular impurities. Consequently, significant materials research appears necessary before substantial improvements in performance can be achieved over the best commercial alumina candidates.

This trend of increasing absorption with the concentration of secondary phases is demonstrated in the $ZrO_2-Al_2O_3$ material system, where it was shown experimentally that increasingly higher strength with ZrO_2 resulted in a corresponding increase in loss tangent values. In addition, the relatively high dielectric constants observed in this material imply that mixtures with ZrO_2 concentrations above 10-15 v/o are not practical for gyrotron window applications. However, substantial improvements in strength properties can still result in this concentration range, provided that low absorption can be maintained by proper control of the microstructural properties.

The experimental study carried out on low-loss fluids showed that the n-alkanes have millimeter absorption well below the naphthene oils and the fluorocarbon fluids such as FC-43, FC-75 and FC-104. The range of fluid properties (viscosity, density, heat capacity) present in the alkanes offers a wide choice for meeting the requirements in specific window cooling applications.



6.0 REFERENCES

1. W. Ho, "Millimeter-Wave Dielectric Property Measurements of Gyrotron Window Materials," Technical Report ORNL/SUB-83-51926/1 (Rockwell Report No. SC5357.2TR), April 1984.
2. W. Ho, "High Temperature Millimeter-Wave Characterization of the Dielectric Properties of Advanced Window Materials," Final Report, AMMRC TR82-28, Contract No. DAAG46-79-007, Army Material and Mechanic Research Center, May 1982.
3. W.B. Westphal and A. Sils, "Dielectric Constant and Loss Data," Technical Report, AFML-TR-72-39, 1972.
4. W.B. Westphal, "Dielectric Constant and Loss Data," Technical Report, AFML-TR-74-250, Part III, 1977; AFML-TR-74-250, Part IV (1980).
5. M.N. Afsar and K.J. Button, "Digest of Millimeter and Submillimeter-Wave Materials Information and Measurements," Millimeter and Submillimeter-Wave Materials Information Measurement Center, 1983.
6. G.A. Slack, General Electric Technical Information Series, Report TIS78-SDR-2199, May 15, 1978.
7. U. Stumper, "Dielectric Absorption of Liquid Normal Alkanes in the Microwave and Far-Infrared Regions, Advances in Molecular Relaxation Processes 7, 189 (1975).



ORNL/SUB/83-51926/2
SC5357.4FR

INTERNAL DISTRIBUTION

- | | | | |
|------|------------------|--------|----------------------------------|
| 1. | P.F. Becher | 12. | J.L. Scott |
| 2. | T.S. Beiglow | 13. | J.M. Spicer, ORNL Patent Office |
| 3. | H.H. Haselton | 14. | T.L. White |
| 4. | H.D. Kimrey, Jr. | 15. | F.W. Wiffen |
| 5. | R.P. Jernigan | 16-17. | Laboratory Records Dept. |
| 6-8. | G.R. Haste | 18. | Laboratory Records, ORNL-RC |
| 9. | H.C. McCurdy | 19. | Y-12 Document Reference Section |
| 10. | D.H. Metzler | 20-21. | Central Research Library |
| 11. | O.B. Morgan, Jr. | 22. | Fusion Energy Division Library |
| | | 23. | Fusion Energy Div., Comm, Center |

EXTERNAL DISTRIBUTION

24. D.S. Beard, Component Branch, Office of Fusion Energy, DoE, ER-531, TGN, Washington, D.C. 20545
25. H. Bennett, Code 38101, U.S. Naval Weapons Center, China Lake, CA 93555
26. L.J. Craig, Varian Associates, 611 Hansen Way, MS B-118, Palo Alto, CA 94303
27. K.J. Button, Francis Bitter Nat'l. Lab, MIT, Cambridge, MA 02139
28. R.A. Dandl, 1122 Calle De Los Serranos, San Marcos, CA 92069
29. J.F. Decker, Office of Fusion Energy, DoE, APP, Rm. 219, ER-54, GTN, Washington, D.C. 20545
30. N. Dionne, Raytheon Co., Foundry Ave., Waltham, MA 02254
31. W.P. Ernst, Princeton Univ., Plasma Physics Lab, PO Box 451, Princeton, NJ 08540
32. D. Evans, AFAL/MLPS Wright-Patterson AFB, OH 45433
33. M.K. Ferber, 203, Dept. of Ceramic Engineering, 105 So. Goodwin Ave., Univ. of Illinois, Urbana, IL 61801
34. P. Ferguson, JAYCOR, 39510 Paseo Padre Parkway, Suite 310, Fremont, CA 94537
35. J.D. Fowler, Los Alamos, Nat'l. Lab., MS-546, Los Alamos, NM 87545
36. J. Fuller, Eng'g Experiment Sta, GA Inst. of Tech., Atlanta, GA 30332



37. T.V. George, Office of Fusion Energy (ETM), DoE, 19901 Germantown Rd., Germantown, MD 20767
38. T. Godlove, Particle Beam Program, Office of Inertial Fusion, DoE, Mail Stop C-404, Washington, D.C. 20545
39. V.L. Granatstein, Dept. of Electrical Engineering, Univ. of Maryland, College Park, MD 20742
40. C. Greskovich, General Electric Co., Corporate R&D, Schenectady, NY 12301
41. G.M. Hass, Component Development, Office of Fusion Energy, DoE, ER-531, GTN, Washington, DC. 20545
42. M. Haas, Naval Research Lab., Washington, D.C. 20545
43. G.W. Hamilton, Reactor Design, MFE Program, Lawrence Livermore National, L6-44, PO Box 5511, Livermore, CA 94550
44. T.M. Hartnett, Raytheon Res. Div., 131 Spring St., Lexington, MA 01273
45. J.L. Hirshfield, Yale Univ., Dept. of Eng. and Applied Science, PO Box 2159, Yale Sta., New Haven, CT 06550
46. D.B. Hopkins, Lawrence/Berkeley Lab., Bldg. 46S, Berkeley, CA 94720
47. H.R. Jory, Varian Assoc., 611 Hansen Way, MS-B109, Palo Alto, CA 94303
48. R.N. Katz, Ceramic Res. Div., Army Materials & Mechanics Res. Center, Arsenal St., Watertown, MA 02172
49. K. Krause, Lawrence Livermore Nat'l. Lab., PO Box 808/L-634, Livermore, CA 94550
50. J.V. Lebacqz, Stanford Linear Accelerator Center, PO Box 4349, Bin 30, Stanford, CA 94305
51. W. Lindquist, Electronics Eng. Dept., Lawrence Livermore Lab, PO Box 808/L-443, Livermore, CA 94550
52. W.T. Messick, Naval Surface Weapons Center, White Oak Lab., Silver Springs, MD 20910
53. H. Mizuhara, GTE/Wesgo, 477 Harbor Blvd., Belmont, CA 94002
54. C. Moeller, General Atomic Co., PO Box 81608, San Diego, CA 92138



ORNL/SUB/83-51926/2
SC5357.4FR

55. G.F. Pierce, 53 Lomond Dr., Inverness, IL 60067
56. R. Pohanka, ONR, Code 471, 800 N. Quincey, Arlington, VA 22217
57. R. Prater, G.A. Technologies, Inc., Fusion and Advanced Technology, P.O. Box 85608, San Diego, CA 92138
58. C.L. Quackenbush, GTE Labs., 40 Sylvan Rd., Waltham, MA 02254
59. B.H. Quon, TRW Defense & Space Systems, 1 Space Park, Bldg. R-1, Redondo Beach, CA 90278
60. M.E. Read, Naval Research Lab, 4556 Overlook Ave. SW, Code 4700, Washington, DC 20375
61. R. Rice, Naval Research Lab, 4556 Overlook Ave. SW, Code 6360, Washington, DC 20375
62. T. Roemesser, TRW Defense & Space Systems, 1 Space Park, Bldg. R-1, Redondo Beach, CA 90278
63. F. Schmid, Crystal Systems Inc., 35 Congress St., Salem, MA 01970
64. G. Simonis, Harry Diamond Lab Branch 13200, 2800 Powder Mill Rd., Adelphi, MD 20783
65. M.S. Sparks, Scientific Res. Center, 9507 High Ridge Pl., Beverly Hills, CA 90210
66. B. Stallard, Lawrence Livermore Lab, PO Box 808, Livermore, CA 94550
67. H.S. Staten, Office of Fusion Energy (ETM), DoE, ER-531, GTN, Washington, DC 20545
68. M.A. Stroschio, AFOSR, Bolling AFB, Washington, DC 20332
69. P.J. Tallerico, AT-5, Accelerator Tech. Div., Los Alamos Scientific Lab, Mail Stop H827, PO Box 1663, Los Alamos, NM 87545
70. J.J. Tancredi, P.O. Box 2999, Electron Dynamics Div., Hughes Aircraft Co., 3100 W. Lomita Blve, Torrance, CA 90509
71. R.J. Temkin, Nat. Magnet Lab, MIT, 170 Albany St., NW16-254, Cambridge, MA 02139
72. D. Wirth, Coors Porcelain Co., R&D, Golden, CO 80401



Rockwell International
Science Center

ORNL/SUB/83-51926/2
SC5357.4FR

73. R. Zacharaia, AFAL/DHM, Wright-Patterson AFB, OH 45433
74. Director, U.S. Army Ballistic Missile Defense Advance Tech. Center,
Attn: D. Schenk, ATC-r, PO Box 1500, Huntsville, AL 35807
75. DoE Technical Information Center, Oak Ridge, TN 37830
76. RADC/OCTP, Griffiss AFB, NY 13441
77. Office of Asst. Manager for Energy R&D, Oak Ridge Operations Office,
DoE, Oak Ridge, TN 37830